Inorganic Chemistry
Article

Inorg. Chem. **2011**, *50*, 213–219 **213**
DOI: 10.1021/ic101783z

Synthesis, Crystal Structure, and Electron Paramagnetic Resonance Investigations of Heteronuclear Co^{II}/Zn^{II} and Co^{II}/Cd^{II} Coordination Polymers

Daniel Lässig, Jörg Lincke, Jan Griebel, Reinhard Kirmse, and Harald Krautscheid*

Fakultät für Chemie und Mineralogie, Universität Leipzig, Johannisallee 29, D-04103 Leipzig, Germany

Received September 1, 2010

The crystal structures of five new Co^{II}, Zn^{II}, and Cd^{II} coordination polymers based on pyridine-substituted triazolyl carboxylates are reported. The two isomorphous compounds $^3_\infty$[M(Me-3py-*p*ba)$_2$] (M = Zn, Co) possess $\{6^6\}$ topology (**dia**). In order to obtain heteronuclear compounds, we synthesized Co^{II}-substituted Zn^{II} and Cd^{II} coordination polymers. At T = 5 K, the powder samples of the diamagnetically diluted Co^{II}/Zn^{II} and Co^{II}/Cd^{II} systems [Co/(Zn,Cd) ≈ 0.01] show intense electron paramagnetic resonance spectra, which were analyzed with an effective spin of $S' = {}^1/_2$. The **g** tensor as well as the ^{59}Co hyperfine tensor $\mathbf{A}^{Co}$ are strongly anisotropic. The **g** tensor components are used to gain information about the symmetry of the Co^{II} coordination sphere and covalency effects. Differential thermal analysis/thermogravimetry−mass spectrometry and temperature-dependent powder X-ray diffraction studies reveal high thermal stability of the three-dimensional coordination polymers up to 390 °C.

Introduction

Microporous coordination polymers, also known as metal−organic frameworks (MOFs), have gained increasing interest in the past decade especially for adsorption studies and potential applications as heterogeneous catalysts.[1−6] Because of the crystallinity of these materials, they possess a definite pore-size distribution. The potential of MOFs as porous solids has been impressively shown by the MIL series and HKUST-1 [Cu_3(btc)$_2$; btc = 1,3,5-benzenetricarboxylate].[1,7] Therein the usage of pure carboxylate ligands as linkers has already been extensively studied.

Apart from carboxylates, nitrogen-containing heterocycles such as pyridines, pyrazoles, 1,2,4-triazoles, and tetrazoles were found to possess promising coordination chemistry for the synthesis of MOFs.[8−11] MOFs with N-donor ligands display interesting properties for heterogeneous catalysis, as can been seen from the cobalt-containing coordination polymer MFU-1.[4] In addition, mixed-metal MOFs, further on described as heteronuclear, display interesting features: the combination of metal ions with different sizes, coordination behavior, and catalytic activity. Principally, there are two strategies for the synthesis of heteronuclear MOFs. This can be achieved by a network with separate positions occupied by different metal ions or by a network with a single position statistically occupied by various metal ions. Recent examples are [Cu_2V_2-F_6O_2(tr$_2$eth)$_2$]$_n$ [tr$_2$eth = 1,2-bis(1,2,4-triazol-4-yl)ethane],[12] [{Cd(NO$_3$)$_2$}$_2$-{(Cu(Pyac)$_2$}$_3$] [Pyac = 3-(4-pyridyl)pentane-2,4-dionato],[13] and [L_MZn]·2DMF·4H$_2$O (L_M = {M[4,4′-(HO$_2$C)$_2$-bpy]$_2$bpy}$^{2+}$, where M = Ru or Os).[14] Hence, in order to synthesize new coordination polymers, we used a recently

Scheme 1. (Me-3py-*p*ba)$^-$ (left) and (Me-4py-*p*ba)$^-$ (right)

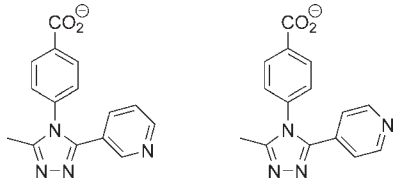

*To whom correspondence should be addressed. E-mail: Krautscheid@rz.uni-leipzig.de.

(1) Chui, S. S.-Y.; Lo, S. M.-F.; Charmant, J. P. H.; Orpen, A. G.; Williams, I. D. *Science* **1999**, *283*, 1148–1150.
(2) Hartmann, M.; Kunz, S.; Himsl, D.; Tangermann, O.; Ernst, S.; Wagener, A. *Langmuir* **2008**, *24*, 8634–8642.
(3) Lua, Y.; Tonigold, M.; Bredenkötter, B.; Volkmer, D.; Hitzbleck, J.; Langstein, G. *Z. Anorg. Allg. Chem.* **2008**, *634*, 2411–2417.
(4) Tonigold, M.; Lu, Y.; Bredenkötter, B.; Rieger, B.; Bahnmüller, S.; Hitzbleck, J.; Langstein, G.; Volkmer, D. *Angew. Chem., Int. Ed.* **2009**, *48*, 7546–7550.
(5) Klein, N.; Senkovska, I.; Gedrich, K.; Stoeck, U.; Henschel, A.; Mueller, U.; Kaskel, S. *Angew. Chem., Int. Ed.* **2009**, *48*, 9954–9957.
(6) Moellmer, J.; Celer, E. B.; Lübke, R.; Cairns, A. J.; Staudt, R.; Eddaoudi, M.; Thommes, M. *Microporous Mesoporous Mater.* **2010**, *129*, 345–353.
(7) Férey, G.; Mellot-Draznieks, C.; Serre, C.; Millange, F.; Dutour, J.; Surblé, S.; Margiolaki, I. *Science* **2005**, *309*, 2040–2042.
(8) Klingele, M. H.; Brooker, S. *Coord. Chem. Rev.* **2003**, *241*, 219.
(9) Beckmann, U.; Brooker, S. *Coord. Chem. Rev.* **2003**, *245*, 17.
(10) Haasnoot, G. *Coord. Chem. Rev.* **2000**, *200*, 131.
(11) Hunger, J.; Krautscheid, H.; Sieler, J. *Cryst. Growth Des.* **2009**, *9*, 4613–4625.
(12) Sharga, O. V.; Lysenko, A. B.; Krautscheid, H.; Domasevitch, K. V. *Acta Crystallogr.* **2010**, *C66*, m269–m272.
(13) Chen, B.; Fronczek, F. R.; Maverick, A. W. *Inorg. Chem.* **2010**, *43*, 8209–8211.
(14) Kent, C. A.; Mehl, B. P.; Ma, L.; Papanikolas, J. M.; Meyer, T. J.; Lin, W. *J. Am. Chem. Soc.* **2010**, *132*, 12767–12769.

Published on Web 12/01/2010

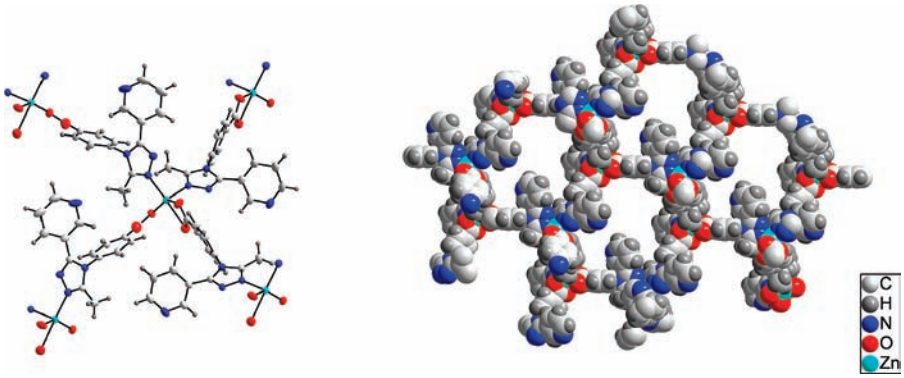

Figure 1. Structural motif (50% ellipsoids, left) and 3D projection of a single net of **1** (right).

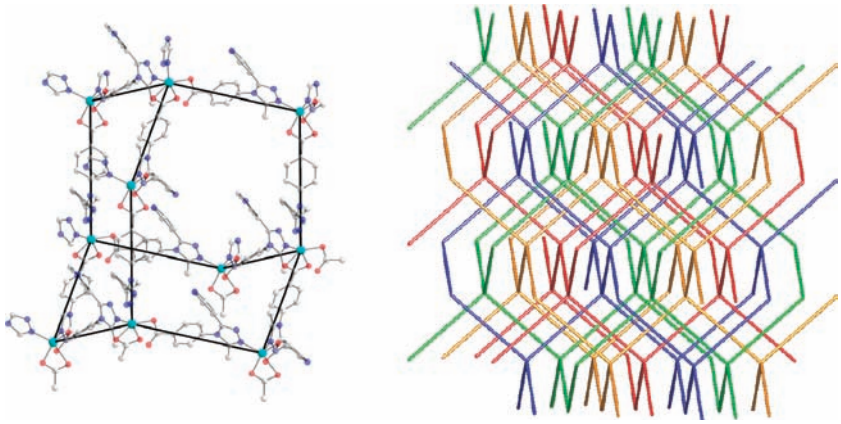

Figure 2. Adamantane backbone showing the $\{6^6\}$ network topology related to diamond (left) and the four interpenetrating networks of **1** (right).

presented series of pyridine-substituted triazolyl benzoates as ligands with multiple binding sites (Scheme 1).[15,16]

On the basis of the ligands 4-[3-methyl-5-(pyridin-3-yl)- and 4-[3-methyl-5-(pyridin-4-yl)-1,2,4-triazol-4-yl]benzoate (Me-3py-*p*ba$^-$ and Me-4py-*p*ba$^-$; Scheme 1), we herein present five new zinc, cadmium, and cobalt coordination polymers. Furthermore, we partially substituted the diamagnetic zinc and cadmium ions by small percentages of paramagnetic Co^{II} ions that might be of interest toward heterogeneous catalysis.[4] The Co^{II}-doped Zn^{II} and Cd^{II} compounds were studied by electron paramagnetic resonance (EPR) in order to gain information about the symmetry of the Co^{II} centers and the covalency of the cobalt−ligand bonds.

Synthesis and Characterization of $^3_\infty$[M(Me-3py-*p*ba)$_2$] [M = Zn (1), Co (2)]

Single crystals of the three-dimensional (3D) coordination polymer **1** were obtained by solvothermal synthesis by reacting zinc(II) acetate with H(Me-3py-*p*ba). The crystal structure was elucidated by means of single-crystal X-ray structure analysis. A microcrystalline powder of **1** was obtained by reaction in ethanol under reflux for 48 h. Compound **1** crystallizes in the noncentrosymmetric, monoclinic space group *Pc* (No. 7) with two formula units per unit cell. The 4-fold-connecting zinc ions in **1** are distorted square-pyramidally coordinated by two triazole rings, a monodentate, and a chelating carboxylate group, leading to a network with $\{6^6\}$ topology (**dia**) related to diamond (Figure 1).[17]

As a result, each net of **1** possesses a 3D pore system that is drastically reduced by 4-fold interpenetration (Figure 2). The remaining solvent-accessible void was calculated to be only 4%.[18] Weak $\pi-\pi$ interactions with a distance of 370 pm between pyridine rings of ligands in neighboring nets are observed, which might be one driving force for the interpenetration.[19]

According to temperature-dependent powder X-ray diffraction (PXRD) data, **1** is thermally stable up to 390 °C (cf. the Supporting Information). The fact that there is no phase transition displays the rigidity of the framework. Differential thermal analysis/thermogravimetry−mass spectrometry (DTA/TG−MS) measurements confirm this high thermal stability, which is probably caused by interpenetration and the dense packing.

PXRD studies reveal the phase purity of the polycrystalline product and show a good agreement between the experimental and simulated patterns based on the single-crystal structure determination (Figure 3).

The isomorphous Co^{II} framework **2** was obtained by reacting cobalt chloride hexahydrate and H(Me-3py-*p*ba) under solvothermal conditions in *N*,*N*-dimethylformamide (DMF). In contrast to the zinc ion in **1**, which can be described as square-pyramidally coordinated, the cobalt ion in **2**

(15) Lässig, D.; Lincke, J.; Krautscheid, H. *Tetrahedron Lett*. **2010**, *51*, 653–656.
(16) Lincke, J.; Lässig, D.; Krautscheid, H. *Acta Crystallogr*. **2009**, *C65*, m488–m490.
(17) *TOPOS*: Blatov, V. A.; Shevchenko, A. P.; Serezhkin, V. N. *J. Appl. Crystallogr*. **2000**, *33*, 1193.
(18) *PLATON*: Spek, A. L. *J. Appl. Crystallogr*. **2003**, *36*, 7–13.
(19) Meyer, E. A.; Castellano, R. K.; Diederich, F. *Angew. Chem., Int. Ed*. **2003**, *42*, 1210–1250.

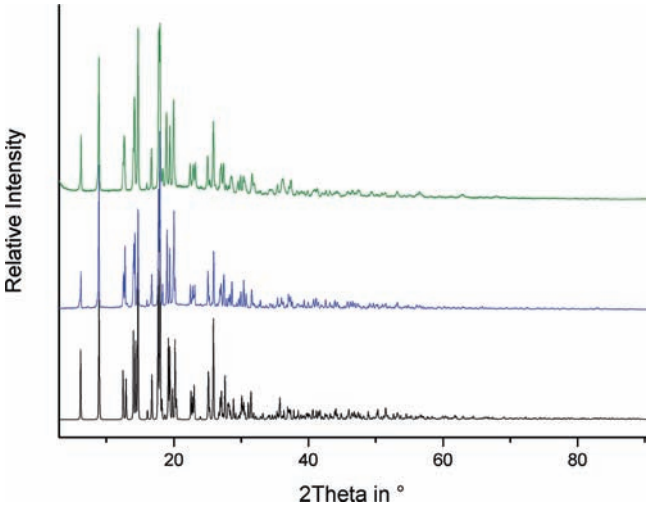

Figure 3. Comparison of the PXRD patterns of a microcrystalline sample (top) and of milled single crystals (middle) and the simulated PXRD pattern of 1 (bottom) based on single-crystal data at 180 K.

Table 1. Selected Bond Lengths and Angles of **1** and **2**[a]

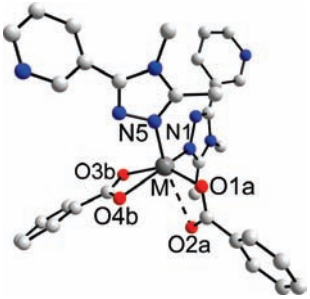

1		**2**	
atoms 1−2	*d*(1,2) [pm]	atoms 1−2	*d*(1,2) [pm]
Zn1−N1	206.9(3)	Co1−N1	208.1(3)
Zn1−N5	204.7(2)	Co1−N5	207.9(3)
Zn1−O1a	199.2(2)	Co1−O1a	204.9(3)
Zn1···O2a	264.9(3)	Co1−O2a	234.1(3)
Zn1−O3b	208.2(2)	Co1−O3b	215.8(3)
Zn1−O4b	228.6(2)	Co1−O4b	214.3(3)
1		**2**	
atoms 1−2−3	angle [deg]	atoms 1−2−3	angle [deg]
N1−Zn1−N5	102.5(1)	N1−Co1−N5	99.4(1)
N1−Zn1−O1a	105.7(1)	N1−Co1−O1a	105.9(1)
N1−Zn1−O3b	92.9(1)	N1−Co1−O3b	91.0(1)
N5−Zn1−O3b	105.47(9)	N5−Co1−O3b	97.4(1)
O1a−Zn1−O3b	146.7(1)	O1a−Co1-O3b	158.2(1)
O1a−Zn1−O4b	94.50(9)	O1a−Co1−O4b	99.5(1)
O2a−Zn1−O4b	81.37(9)	O2a−Co1−O4b	85.5(1)
O2a−Zn1−N5	151.12(9)	O2a−Co1−N5	152.4(1)

[a] Symmetry codes a, $-1+x, 1-y, -0.5+z$; b, $1+x, 2-y, -0.5+z$.

is distorted octahedrally coordinated by two bidentate carboxylates and two triazole units. Table 1 summarizes the selected bond lengths and angles of **1** and **2**.

Microcrystalline **2** was obtained by refluxing the starting materials in DMF for 2 days. The experimental PXRD pattern is in good agreement with the theoretical one simulated from the single-crystal structure data (180 K). As can be seen from the temperature-dependent PXRD and DTA/TG−MS studies, **2** is thermally stable up to 410 °C.

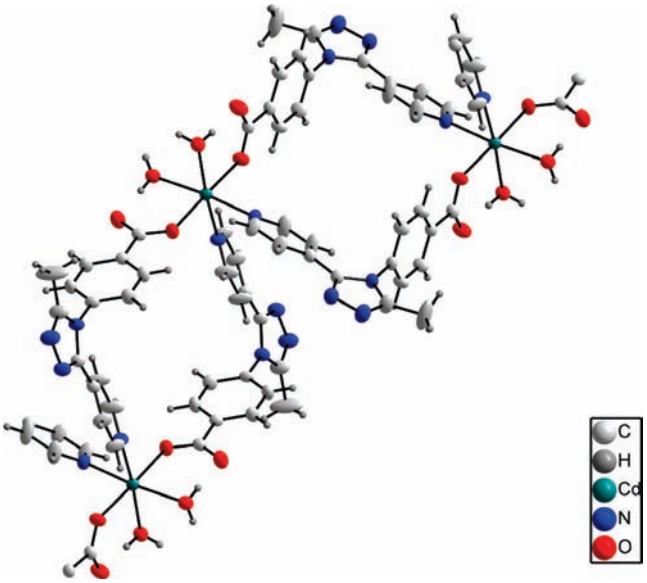

Figure 4. Fragment of the crystal structure of **4** (50% ellipsoids).

Because of the isomorphous crystallization of the coordination polymers **1** and **2**, we investigated the partial substitution of the zinc ions in **1** by cobalt ions in low percentages. The diamagnetically diluted Co^{II} system was found to be suitable for EPR measurements performed in the temperature range of $5 \le T \le 20$ K. Therefore, a series with increasing cobalt concentration in $^{3}_{\infty}[Co_xZn_{1-x}(Me\text{-}3py\text{-}pba)_2]$ ($x = 0.01-0.10$) was synthesized. The PXRD patterns reveal good structural agreement of the synthesized materials.

Synthesis and Characterization of $^{1}_{\infty}[M(Me\text{-}4py\text{-}pba)_2(H_2O)_2]\cdot H_2O$ [M = Zn (3), Cd (4)] and $^{1}_{\infty}[Co(Me\text{-}4py\text{-}pba)_2(H_2O)_2]\cdot 2H_2O\cdot CH_3CN$ (5)

The polymeric chains **3**−**5** were obtained by diffusion methods. Basically, they all possess similar structural motifs. According to the single-crystal structure analyses, **3** and **5** crystallize in the triclinic space group $P\bar{1}$ (No. 2), whereas **4** crystallizes in the monoclinic space group $C2/c$ (No. 15). The metal ions are coordinated by four ligands to form a polymeric chain (Figure 4). In the cases of **3** and **4**, the metal ions are distorted octahedrally coordinated by two monodentate carboxylates of (Me-4py-*p*ba)$^-$ in trans orientation, two pyridine rings in cis position, and two additional water molecules. In contrast, in **5**, the two pyridine rings and the water molecules are arranged in trans position and the Co^{II} ion resides on the inversion center.

Considering the structural motif, intramolecular hydrogen bonding between the noncoordinated carboxylate oxygen atoms of the carboxylate and the aquo ligands is observed. With short O···O distances of about 260 pm, the hydrogen bonds apparently enhance the stability of the coordination polymers (Table 2).

Polycrystalline material obtained by diffusion methods was investigated using PXRD showing a good agreement between the simulated and respective experimental patterns in the case of all three products. Temperature-dependent PXRD shows that all three coordination polymers undergo several phase transitions up to their decomposition temperature of 430 °C in the case of **3** (Figure 5) and **5** and 350 °C in the case of **4**. Despite the fact that the structures of the

Table 2. Selected Bond Lengths and Angles of **3**–**5**[a]

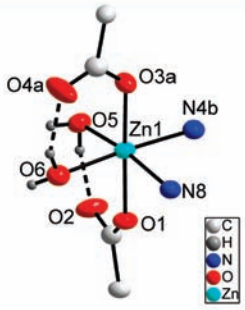

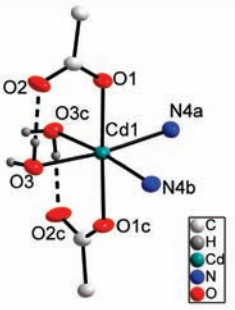

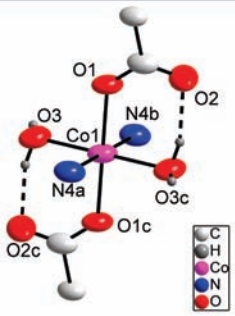

3		4		5	
atoms 1-2	**d (1,2) [pm]**	**atoms 1-2**	**d (1,2) [pm]**	**atoms 1-2**	**d (1,2) [pm]**
Zn1-O1	209.2(4)	Cd1-O1	229.3(1)	Co1-O1	209.7(3)
Zn1-O3a	204.7(4)	Cd1-O3	235.8(2)	Co1-O3	212.1(3)
Zn1-O5	213.0(4)	Cd1-N4a	236.0(2)	Co1-N4a	217.9(4)
Zn1-O6	219.2(4)	O2···O3	261.1(2)	O2···O3c	268.8(4)
Zn1-N8	219.0(4)				
Zn1-N4b	218.0(4)				
O2···O5	265.9(5)				
O4a···O6	260.3(4)				
atoms 1-2-3	**angle [°]**	**atoms 1-2-3**	**angle [°]**	**atoms 1-2-3**	**angle [°]**
O3a-Zn1-O6	92.4(2)	O1-Cd1-O3	87.81(5)	O1-Co1-O3	88.1(1)
O1-Zn1-O6	87.0(2)	O1-Cd1-N4b	93.46(6)	O1-Co1-O3c	91.9(1)
O3a-Zn1-N8	95.3(2)	O3c-Cd1-N4a	94.50(6)	O1-Co1-N4b	91.4(1)
O1-Zn1-N8	81.8(2)	N4b-Cd1-N4a	86.33(9)	O1-Co1-N4a	88.6(1)
O1-Zn1-N4b	91.0(2)	O1-Cd1-N4a	85.25(5)	O3-Co1-N4a	87.1(1)
O3a-Zn1-O5	93.4(2)	O3c-Cd1-O3	85.50(8)	O3-Co1-N4b	92.9(1)

[a] Symmetry codes for **3**: a, $1-x, 1-y, 2-z$; b, $-x, 2-y, 1-z$. Symmetry codes for **4**: a, $-0.5+x, 1.5-y, -0.5+z$; b, $1.5-x, 1.5-y, 1-z$; c, $1-x, y, 0.5-z$. Symmetry codes for **5**: a, $x, y, z-1$; b, $-x, 1-y, 1-z$; c, $-x, 1-y, -z$.

high-temperature phases are unknown, the high thermal stability of these one-dimensional (1D) coordination polymers is remarkable.

DTA/TG–MS measurements display a loss of about 7.5% by weight within two steps until 230 °C in the case of **3**, which correlates well with the loss of three water molecules detected by MS. As can been seen from the temperature-dependent PXRD measurements and DTA, the loss of solvent is connected with endothermic phase transitions. At 330 °C, a third endothermic phase transition without any TG–MS signals is detected (Figure 6). The PXRD pattern of this phase is consistent with the high-temperature phase of **5**. At 430 °C, **3** loses its crystallinity because of decomposition of the material under release of carbon dioxide. The decomposition temperatures of each compound **3**–**5** determined by DTA/TG–MS (Figure 6) correspond to the one determined using temperature-dependent PXRD.

According to magnetic measurements, the Co^{II} ions in **5** are in a *high-spin* state. Because of the structural similarities, we achieved partial substitution of the diamagnetic zinc or cadmium ions in **3** and **4** by small percentages of cobalt. In order to gain structural and bonding information about the

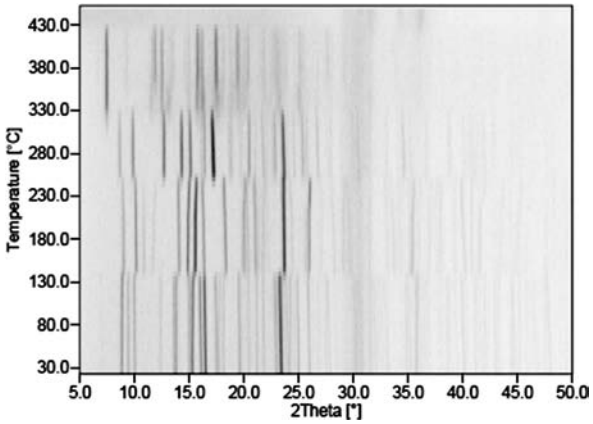

Figure 5. Temperature-dependent PXRD pattern of **3** (Guinier–Simon diagram).

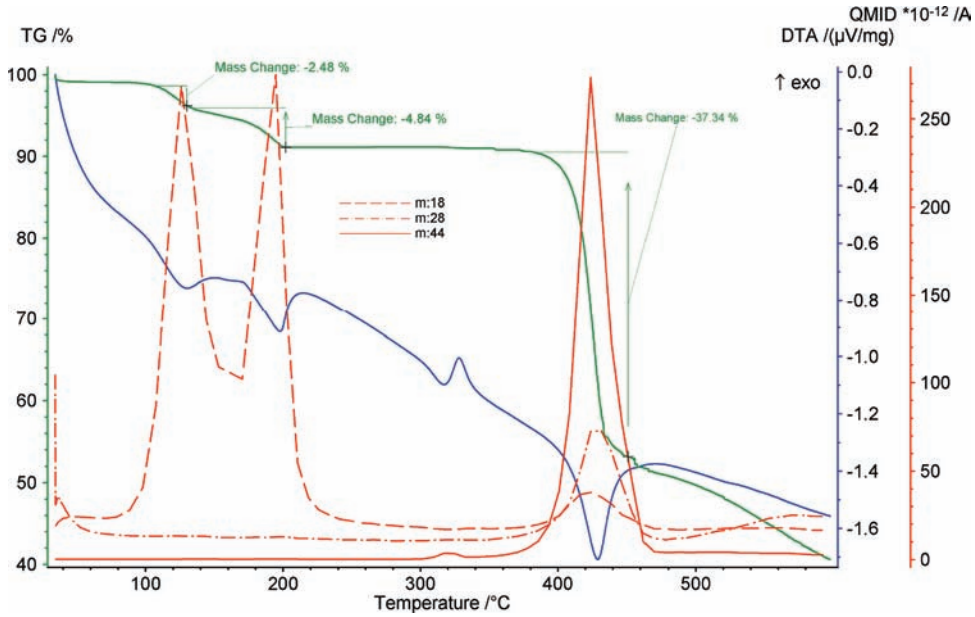

Figure 6. DTA/TG−MS measurement of **3**.

incorporated Co^{II}, X-band EPR investigations have been carried out. Due to the bad solubility of the starting materials in the solvents used for synthesis, suitable diamagnetically diluted single crystals could not be prepared for the EPR measurements. Therefore powder samples of the Zn^{II}-based framework **1** and of the Zn^{II} and Cd^{II} coordination polymers **3** and **4** doped with Co^{II} were used. The Co/(Zn,Cd) ratio was chosen to be 0.01 because, for higher Co^{II} concentrations, line-broadening effects were observed, leading to a lower quality of the spectra. In all cases, at temperatures in the range 5−20 K, strong EPR signals were obtained. Low temperatures are required because of short spin−lattice relaxation times. The EPR spectra of Co^{II} doped into **1**, **3**, and **4** are shown in Figure 7, together with their simulations.

At zero magnetic field, according to Abragam and Pryce[20] for Co^{II} $3d^7$ in an octahedral ligand field, the lowest-lying orbital triplet (labeled Γ_4) splits into a doublet, a quartet, and a sextet, with the doublet lying lowest. Resonance is observed only for the lowest doublet, which is several hundred reciprocal centimeters below the first excited state. Further on, the large amount of orbital angular momentum in the Γ_4 triplet leads to a ground state g value of 4.3, which differs noticeably from 2.0023. Lower ligand-field symmetries, as present in our compounds, cause further splittings of the levels. However, the resonance, as before, is observed only in the lowest Kramers doublet. The **g** tensor components are now observed in a range from 1.5 to 8.

Because of an effective spin of $S' = {}^1/_2$ of the ground-state doublet, the spectra can be analyzed with the following spin Hamiltonian:

$$H = \sum_{i=x,y,z} (\mu_B g_i' B_i S_i' + A_i' S_i' I_i) \qquad (1)$$

where the second term represents the nuclear hyperfine interaction with the ^{59}Co nucleus ($I = {}^7/_2$). Usually, this interaction is resolved in the low-field g region but not for the other two g values. This has been found in this work for Co^{II} in the host lattices **1** and **4** (Figure 7a,c) but not for Co^{II} in the Zn^{II} lattice **3** (Figure 7b). In this rare case, the ^{59}Co hyperfine structure is resolved for all three g features. This indicates a nearly perfect incorporation of the guest complex into the host lattice, preventing g strain effects.

The tensor components of **g** and $\mathbf{A}^{Co}$ have been obtained by simulation of the EPR spectra using the program package *EasySpin*[21] and an effective spin of $S' = {}^1/_2$. The linewidths used are given in Figure 7. Several attempts have been made to simulate the spectra with $S' = {}^3/_2$ and large values for the fine structure tensor **D**. In this case, however, nine parameters have to be adjusted, and we got no unambiguous solution. The results are listed in Table 3, together with the single-crystal data reported for Co^{II} doped into ZnF_2.

The spectra obtained are characterized by a very large **g** tensor anisotropy, indicating a strong influence of the spin−orbit coupling. Also, the ^{59}Co hyperfine structure tensor shows a pronounced anisotropy.

According to Tinkham,[22] the **g** tensor components for distorted octahedral Co^{II} complexes accurate to first order are written in the form $g_i = (g_S)_i + k(g_L{}^0)_i$, where (g_S) and $k(g_L{}^0)$ stand for the spin and orbital contributions, respectively. The individual tensor components are given in the following equations:

$$g_x' = \left[\frac{10}{3} - \frac{8}{3}a\right] + k(1-2a)$$

$$g_y' = \left[\frac{10}{3} + \frac{4}{3}a + \frac{4}{3}r\right] + k(1+a+r) \qquad (2)$$

$$g_z' = \left[\frac{10}{3} + \frac{4}{3}a - \frac{4}{3}r\right] + k(1+a-r)$$

The average g value, $\langle g \rangle$, is expressed by

$$\langle g \rangle = \frac{10}{3} + k \qquad (3)$$

(20) Abragam, A.; Pryce, M. H. L. *Proc. R. Soc. London* **1951**, *A 206*, 173–191.

(21) Stoll, S.; Schweiger, A. *J. Magn. Reson.* **2006**, *178*, 42–55.

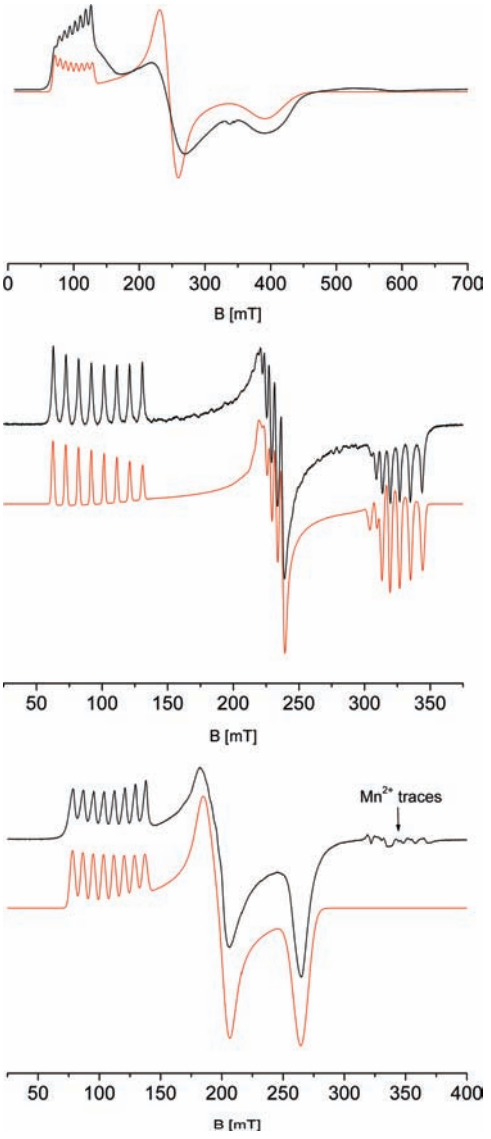

Figure 7. Experimental X-band EPR spectra (black, $T = 5$ K) of Co^{2+} in **1** (a), **3** (b), and **4** (c) and their simulations (red). The linewidths [MHz] for the simulations are (in the order x, y, z): (a) 1300, 650, 800, (b) 75, 160, 135, and (c) 450, 380, 500.

In these equations, a represents the axial term and r the rhombic component of the ligand field. Contributions of the excited ^4P term are not included. However, covalency is allowed via the orbital reduction factor k.

The estimated values for a, r, and k are given in Table 3, together with the estimated values for the spin and orbital contributions $(g_S)_i$ and $k(g_L^0)_i$. The latter ones indicate strong orbital contributions especially for the y component of **g**. The values obtained for a, r, and k allow some further conclusions within the simple model applied: In the zinc lattice of **3**, the first coordination sphere of Co^{II} appears to be more distorted than that in the cadmium lattice of **4**. This corresponds to the metal−donor atom bond lengths, which are noticeably larger in the Cd^{II} coordination polymer **4** than in the Zn^{II} coordination polymer **3**, resulting in more space for the incorporated Co^{II} ions, which can build a less distorted octahedron. As can be seen from Table 2, in the Zn^{II} coordination polymer **3**, the Zn−donor atom distances are similar to those of the Co^{II} compound **5**.

Table 3. Effective Principal Values[b] of $\mathbf{g}'$ and $\mathbf{A}^{Co}$ as Well as Values for a, r, k, $k(g_S)_i$, and $k(g_L^0)_i$[a]

	host lattice			
	1	**3**	**4**	ZnF_2[22]
g_x'	1.740	2.090	2.611	(2.6)[c]
g_y'	6.850	7.100	6.382	6.05
g_z'	2.800	3.000	3.525	4.1
g_{av}'	3.797	4.063	4.173	4.25
A_x'	100	145	45	(−129.1)[c]
A_y'	780	970	753	650
A_z'	100	100	120	(201)[d]
a	0.57	0.48	0.36	0.38
r	1.12	0.99	0.63	0.44
k	0.47	0.73	0.91	0.90
$k(g_L^0)_x$	−0.07	0.03	0.25	0.22
$k(g_L^0)_y$	1.26	1.80	1.81	1.63
$k(g_L^0)_z$	0.21	0.36	0.66	0.85
$(g_S)_x$	1.81	2.03	2.361	2.33
$(g_S)_y$	5.59	5.30	4.572	4.42
$(g_S)_z$	2.59	2.64	2.865	3.25

[a] Hyperfine coupling parameters are given in megahertz. [b] $g_i' \pm 0.005$; $A_i' \pm 10$. [c] Not observed. [d] Not resolved.

For the Co^{II}/Zn^{II} system, the orbital reduction factor k is smaller than that obtained for the Co^{II}/Cd^{II} system, indicating more covalency for the Co−donor atom bonds in the former system. Also, the spin−orbit contribution is more pronounced for the Co^{II}/Zn^{II} system, as reflected by the larger **g** anisotropy.

For Co^{II} in the coordination polymer **1**, eqs 2 and 3 give no reliable values for r and k. This is expected because in this case the coordination geometry of the incorporated cobalt ions comes closer to the distorted pyramidal arrangement of the zinc ions than to an octahedral one. Obviously, the structure of **1** fully incorporates Co^{II} on Zn^{II} positions.

Conclusion

The crystal structures of the isomorphous coordination polymers $^3_\infty[M(Me\text{-}3py\text{-}pba)_2]$ [M = Zn (**1**), Co (**2**)] have been determined (Table 4). A topological analysis reveals a 4-fold interpenetrated network with $\{6^6\}$ topology (**dia**). Temperature-dependent PXRD and DTA/TG−MS measurements show high thermal stability up to 390 and 420 °C. Therefore, it can be concluded that these coordination polymers with single networks of high porosity stabilize themselves by multiple interpenetrations. Additionally, the diamagnetically diluted compounds $^3_\infty[Co_xZn_{1-x}(Me\text{-}3py\text{-}pba)_2]$ ($x = 0.01-0.10$) were synthesized and characterized using X-band EPR spectroscopy.

Furthermore, we synthesized three 1D coordination polymers **3**−**5** possessing similar structural motifs. Temperature-dependent PXRD measurements revealed multiple phase transitions.

In addition, we showed the possibility of the substitution of metal ions in MOFs in low percentages by X-band EPR in diamagnetically diluted Co^{II}/Zn^{II} and Co^{II}/Cd^{II} systems of the coordination polymers **1**, **3**, and **4**. The effective **g** tensors show a pronounced anisotropy. From analysis of the **g** tensor components of Co^{II} in **3** and **4**, the octahedral symmetry of Co^{II} in **3** (Zn^{II} lattice) is found to be more distorted than that in **4** (Cd^{II} lattice). Furthermore, in **3**, the covalency of the Co−donor atom bond is noticeably larger than that in **4**. It could be shown that partial substitution of Zn^{2+} or Cd^{2+} ions by Co^{2+} in coordination polymers could be achieved. Porous

(22) Tinkham, M. *Proc. R. Soc. London* **1956**, *A 236*, 549–563.

Table 4. Crystallographic Data for **1**−**5**[23]

	1	**2**	**3**	**4**	**5**
color and shape	colorless prism	purple prism	colorless prism	colorless prism	orange prism
cryst dimens [mm]	0.39 × 0.42 × 0.44	0.20 × 0.50 × 0.50	0.14 × 0.19 × 0.25	0.25 × 0.36 × 0.50	0.10 × 0.20 × 0.50
formula	$ZnC_{30}H_{22}N_8O_4$	$CoC_{30}H_{22}N_8O_4$	$ZnC_{30}H_{28}N_8O_7$	$CdC_{30}H_{28}N_8O_7$	$CoC_{32}H_{33}N_9O_8$
M [g·mol^{-1}]	623.93	617.49	677.97	725.00	730.60
temperature [K]	180(2)	180(2)	213(2)	213(2)	180(2)
diffractometer	STOE IPDS-2T	STOE IPDS-2T	STOE IPDS-I	STOE IPDS-I	STOE IPDS-2T
cryst syst	monoclinic	monoclinic	triclinic	monoclinic	triclinic
space group	*Pc* (No. 7)	*Pc* (No. 7)	$P\bar{1}$ (No. 2)	*C*2/*c* (No. 15)	$P\bar{1}$ (No. 2)
unit cell					
a [pm]	714.97(6)	704.72(5)	1164.2(2)	2027.7(2)	762.0(2)
b [pm]	1423.58(8)	1419.5(2)	1168.5(2)	1213.9(2)	1108.1(3)
c [pm]	1385.6(2)	1396.8(1)	1362.8(2)	1377.9(1)	1120.0(3)
α [deg]			70.82(1)		68.04(2)
β [deg]	97.792(6)	96.728(6)	70.77(1)	115.050(7)	78.20(2)
γ [deg]			60.90(1)		86.42(2)
V [10^6 pm^3]	1397.3(2)	1387.6(2)	1497.1(4)	3072.4(6)	858.4(4)
Z	2	2	2	4	1
density [g·cm^{-3}]	1.483	1.483	1.504	1.567	1.413
μ(Mo Kα) [mm^{-1}]	0.931	0.673	0.883	0.772	0.563
$\theta_{min}-\theta_{max}$ [deg]	1.15−25.00	1.04−25.00	1.65−25.00	1.90−25.00	1.15−24.00
reflns measd	7490	5511	8944	10803	5061
indep reflns	4447	3816	4960	2700	2650
obsd reflns [$I > 2\sigma(I)$]	4337	3742	2996	2235	1825
R_{int}	0.0321	0.0300	0.0628	0.0244	0.0729
param refined	391	391	437	222	237
R1 [$I > 2\sigma(I)$]	0.0335	0.0358	0.0536	0.0204	0.0556
wR2 (all data)	0.0916	0.0926	0.1362	0.0569	0.1492
Flack x parameter	0.003(8)	0.00(2)			
max/min peak [10^{-6} pm^{-3}]	0.4/−0.5	0.4/−0.3	0.8/−0.5	0.3/−0.1	0.3/−0.4

MOF materials with such substitutions might be particularly interesting concerning heterogeneous catalysis.

Acknowledgment. We thank M.Sc. Florian Kettner for DTA/TG−MS analyses and M.Sc. Dirk Friedrich for his assistance with the atomic absorption spectroscopy measurements. Financial support by Deutsche Forschungsgemeinschaft (DFG SPP 1362 - Poröse metallorganische Gerüstverbindungen), University of Leipzig (PbF-1), and the graduate school BuildMoNa is gratefully acknowledged. D.L. acknowledges the fellowship of the Fonds der Chemischen Industrie and J.L. acknowledges the ESF fellowship.

(23) Sheldrick, G. M. *Acta Crystallogr.* **2008**, *A64*, 112–122.

Supporting Information Available: Experimental details associated with this paper. This material is available free of charge via the Internet at http://pubs.acs.org. CCDC 783568−783572 contain the supplementary crystallographic data for this paper. These data can be obtained free of charge from the Cambridge Crystallographic Data Centre via www.ccdc.cam.ac.uk/data_request/cif.